ORIGINAL RESEARCH ARTICLE

Experimental Phase Equilibria and Liquidus of $CaO-Al_2O_3-SiO_2-Na_2O-B_2O_3$ Slags Relevant to E-waste Processing

MD KHAIRUL ISLAM, MICHAEL SOMERVILLE, MARK I. POWNCEBY, JAMES TARDIO, SURESH BHARGAVA, and NAWSHAD HAQUE

Ternary master slags based on the $CaO-Al_2O_3-SiO_2$ system with CaO/SiO_2 (C/S) ratio 0.3–1.0 were doped with 5–20 wt pct of anhydrous borax ($Na_2B_4O_7$) to study the phase equilibria of the quinary $CaO-Al_2O_3-SiO_2-Na_2O-B_2O_3$ slag system within the temperature range 1050–1350 °C. This research uses the well-known method of high temperature equilibration of slags followed by rapid quenching. The quenched slag samples were examined using a Scanning Electron Microscope (SEM) and Wavelength Dispersive Electron Probe Microanalysis (WD-EPMA) technique to determine the structure and to analyse the chemistry of the phases in equilibrium. The primary phase of 15 slag compositions was identified and the liquidus temperature of the slags were determined within an uncertainty range of ±10–20 °C by using an iterative approach. Overall, the liquidus temperature of slags decreased with increasing borax content with the highest liquidus reduction observed in slags having a C/S ratio 0.3 and the lowest in the slag series with C/S ratio of 1.0. A comparative analysis of the effect of borax, Na_2O and B_2O_3 on the liquidus temperature of slags is discussed. Results indicated that although borax reduces the liquidus of ternary $CaO-Al_2O_3-SiO_2$ slags, the addition of B_2O_3 individually showed more prominent effects than borax in reducing the slag liquidus. Anorthite ($CaO.Al_2O_3.2SiO_2$), pseudowollastonite ($CaO.SiO_2$) and gehlenite ($2CaO.Al_2O_3.SiO_2$) primary phases were identified.

https://doi.org/10.1007/s11663-023-02952-9

I. INTRODUCTION

ELECTRONIC waste (e-waste) is generated from discarded electronic equipment and electrical appliances when they reach their end-of-life and no longer have an appeal to the consumer. It is one of the major waste streams of the current world with an annual generation of more than 50 Mt globally.[1] Moreover, the volume of e-waste generation is increasing rapidly at a rate of 3–5 wt pct annually.[1,2] The proper disposal and management of this waste stream has two main motivations (a) saving the environment from the detrimental effect of the hazardous substances contained in e-waste and (b) recovery of valuable materials which can potentially be used in further manufacturing leading towards a circular economy.[3–5] While there is no doubt of the importance of recovering materials from e-waste, the choice of routes which optimise the environmental and economic factors is still challenging for many reasons including the heterogeneity, chemistry, and complex structures of e-waste components.[6,7]

To recover valuable metals from e-waste, various reprocessing techniques have been considered, including physical separation and pyrometallurgical and hydrometallurgical methods, operating either in isolation or in combination.[8–10] Among these methods, smelting e-waste in an existing primary copper smelter is the most advanced and offers several advantages such as rapid processing, the ability to handle high volumes of feed materials, and industrial scalability.[11,12] Although the aforementioned has a lot of advantages and is currently practiced in some areas of the world including

MD KHAIRUL ISLAM is with the Centre for Advanced Materials & Industrial Chemistry (CAMIC), School of Science, RMIT University, GPO Box 2476, Melbourne, VIC, 3001, Australia and with the CSIRO Mineral Resources, Private Bag 10, Clayton South, VIC, 3169, Australia and also with the Bangladesh Council of Scientific and Industrial Research (BCSIR), IMMM, Joypurhat 5900, Bangladesh. Contact e-mail: Khairul.islam@csiro.au. MICHAEL SOMERVILLE and MARK I. POWNCEBY are with the CSIRO Mineral Resources. JAMES TARDIO and SURESH BHARGAVA are with the Centre for Advanced Materials & Industrial Chemistry (CAMIC), School of Science, RMIT University. NAWSHAD HAQUE is with the CSIRO Energy, Private Bag 10, Clayton South, VIC, 3169, Australia.

Manuscript submitted March 9, 2023; accepted October 15, 2023.
Article published online November 10, 2023.

Europe, Canada, China, Japan and South Korea, the question of collection and transportation costs associated with e-waste sourcing can be a major decision-making factor.[13,14] For example, in a large country like Australia, most of the e-waste is generated in the highly populated city areas along the eastern/southeastern coastline. The existing primary copper smelters however are far removed from the capital cities and hence the transportation of the e-waste from the cities to the primary smelters is expensive.[15] A potential alternative could be the establishment of secondary copper or scrap smelting processing units, where copper-based waste materials can be recycled. This method, which is also known as black copper smelting, has been the subject of focused research. For example, a study based on the ternary slag system $CaO\text{-}SiO_2\text{-}FeO_x$ was conducted to investigate the distribution of tin and indium from waste electronics under the conditions of black copper smelting.[16] The authors however concluded that the method may not be suitable for the recovery of all targeted metals. Another method that has been investigated is direct smelting of e-waste, especially printed circuit boards (PCBs) in controlled atmosphere furnaces equipped with specially designed fume extraction and treatment units.[17] A recent pilot scale study by Nicol et al (2023) investigated the recovery of critical metals from e-waste using ISASMELT^{TM} Technology which reinforces the dominance of pyrometallurgical processing of e-waste scraps.[18] In these systems, some potential challenges are inevitable since there are significant amounts of Al_2O_3, SiO_2 and CaO in the slag phase obtained after melting e-waste.[12,19] The presence of high CaO, SiO_2 and Al_2O_3 will increase the temperature required to create a liquid slag phase (above 1400 °C) which leads to higher energy consumption. In this regard, efficient fluxing could reduce the liquidus (*i.e.*, melting) temperature of the $CaO\text{-}Al_2O_3\text{-}SiO_2$ system to a lower temperature. As a flux FeO might be a potential candidate, and the $FeO/Fe_2O_3\text{-}SiO_2\text{-}Al_2O_3\text{-}CaO$ system has previously been extensively studied. Similarly, limestone ($CaCO_3$), dolomite [$CaMg(CO_3)_2$], fluorspar (CaF_2) and borax ($Na_2B_4O_7$) are all used as fluxes in metallurgical processing[20] and for e-waste PCB smelting, since the PCB slag contains significant amount of CaO, CaO is a fluxing agent in the slag system. In secondary copper processing SiO_2 is also used as flux to form a liquid slag targeting a specific primary phase field with a reasonable viscosity.[18] An optimum fluxing condition could be found by a rigorous experimental investigation targeted at defining the conditions required for attaining the lowest practicable liquidus temperature.

Borax has long been used in metallurgical industries as a flux to reduce the melting temperature of metals and alloys, in refining to remove oxide impurities from metals, during brazing of non-ferrous metals and alloys, welding of steels, and in jewellery industries.[21–23] Borax can be decomposed to Na_2O and B_2O_3 at high temperatures and therefore the presence of both Na_2O and B_2O_3 fluxes could be examined in a slag system as the effect of these two fluxes, individually, as has been discussed in previous articles.[24,25] In other studies, carbothermic reduction of ilmenite ores was conducted with the addition of borax to lower the reduction temperature and to increase the reduction rate of ilmenite.[26] It has also been recently used in extracting nickel and cobalt by smelting laterite ores where borax was used as a flux along with Na_2CO_3 to obtain the highest metal recovery and a high-grade nickel matte at a relatively lower smelting temperature.[27] The application of borax as a fluxing agent in the utilisation of high titania blast furnace slags to produce a sintered foamed glass-ceramic is also notable. Moreover, the manufacturing of geopolymer utilising metallurgical processing by-products obtained from blast furnace slag, electric arc furnace slag, and ladle slags have been widely investigated.[28–30] While borax was reported to improve the thermomechanical properties of the geopolymer in,[30] a common finding that was reported in each of the aforementioned studies was the lowering of the liquidus or characteristic temperatures (*i.e.*, sintering temperature, softening temperature) of the systems studied by adding borax as a flux additive.[30,31]

Inspired by the applications of borax as a flux in a range of areas including steel making and smelting it was decided to investigate the effect of borax on the $CaO\text{-}Al_2O_3\text{-}SiO_2$ slag system that could be suitable for smelting of e-waste printed circuit boards (PCBs). The application of Na and B fluxes in real industrial processing is evident at US Borax, a company that is part of Rio Tinto. They employ several industrial-scale applications of borax, including its use in copper (Cu), aluminum (Al), nickel (Ni), and lead (Pb) metallurgy. The Na and B fluxes are employed in these processes to facilitate various chemical reactions and promote efficient metal extraction and refining in large-scale industrial operations.[32] Borax could potentially be used in the pyrometallurgical processing of e-waste PCBs to reduce the operating temperature and form a liquid slag that allows the metals to transport through the liquid slag to form a copper-rich alloy in the bottom of the crucible.[33,34] The use of these fluxes lowers the liquidus temperature of slags, which can affect the refractory lining's lifespan in reaction vessels through various mechanisms, such as chemical reactions, penetration through pores causing cracks, and erosion. Thus, the use of borax as a flux in certain processes can present two main issues. Firstly, it has the potential to cause corrosion of the refractory linings in reactors due to the aggressive nature of the generated slag. However, engineering solutions exist to address these refractory lifetime challenges. One approach is to carefully select refractories that are minimally affected by chemical attacks from the generated slag. For example, high Al_2O_3 refractories have been shown to withstand exposure to Na salts at temperatures up to 900 °C without significant corrosion products.[35] Secondly, under reducing conditions, soda fumes can be generated. Studies in the literature indicate that the evaporation of Na_2O and B_2O_3 increases with higher operating temperatures, higher proportions of Na_2O and B_2O_3, and at greater basicity of the slags in pyrometallurgical processes.[36] However, by incorporating borax flux into the CAS (calcium aluminosilicate) system, it is possible

to lower the operating temperature, resulting in reduced generation of Na_2O fumes. Moreover, with optimal levels of fluxing, evaporation can be minimized at a practical lower temperature. To the best of the author's knowledge there is little understanding on the effect of borax on the liquidus and phase equilibria of slags that can be applied in direct smelting of e-waste PCBs to separate metal alloys from the impurity materials.

II. EXPERIMENTAL

A. *Materials*

Reagent grade oxides and carbonates were used to prepare three master $CaO\text{-}Al_2O_3\text{-}SiO_2$ (CAS) slags of varying CaO/SiO_2 (C/S) ratios and sub-slags by doping the CAS master slags with borax ($Na_2B_4O_7.10H_2O$) at different levels. The source of SiO_2 (99.9 pct) was Sigma-Aldrich, Al_2O_3 (99.5 pct) was purchased from VWR Chemicals. The required amount of CaO was obtained from $CaCO_3$ (99.5 pct) supplied by Sigma-Aldrich and borax (99.9 pct) from Glitz Green, Australia. Platinum alloy crucibles (Pt97 pct/Rh3 pct) supplied by XRF Labware Pty Ltd, Melbourne were used to melt the master and sub-slags in a muffle furnace. Thin platinum foils (0.025 mm thickness) were used to make small capsules to contain the slag samples at higher temperatures inside the tube furnace during the equilibration experiments. Platinum foil was supplied by Cookson Dental, UK.

B. *Equipment and Methods*

1. *Preparation of slags*

Master slags ($CaO\text{-}Al_2O_3\text{-}SiO_2$) and sub-slags ($CaO\text{-}Al_2O_3\text{-}SiO_2\text{-}Na_2O\text{-}B_2O_3$) were prepared by melting pre-weighed mixtures of oxide and carbonate powders in a muffle furnace (Tetlow Kilns and Furnaces, Australia) using a platinum alloy crucible. The powdered master slag was prepared first by melting followed by pulverising and then a calculated amount of borax at different levels (5, 10, 15 and 20 wt pct on an anhydrous basis) was added. The pulverised powder samples were thoroughly mixed and re-melted at 1600 °C. The homogenised, and molten slag was poured in a cold steel channel to quench. Precautions were taken in every experimental step to overcome challenges due to the hygroscopic nature of Na_2O and B_2O_3 doped slags. The prepared slags were always kept in desiccators and under vacuum.

2. *Analysis of bulk slag composition*

To determine the compositions of the three master slags (S100, S200, and S300) as well as the twelve borax-doped sub-slags, X-ray Fluorescence Spectroscopy (XRF) and Inductively Coupled Plasma Optical Emission Spectrometry (ICP-OES) were employed. For XRF analysis, the slag samples were fused with lithium borate to create a uniform glass disc for measurement using the Bruker 4kW S8 Tiger WDXRF instrument. The XRF results were highly accurate, with a precision of approximately 0.5 pct relative, based on calibration data gathered by CSIRO over several years. Due to the challenging nature of boron analysis using XRF, a Varian 730-ES ICP-OES instrument was utilized. To prepare the samples for ICP-OES analysis, the powdered slag samples were digested with a mixture of HNO_3 and HF and heated until complete dissolution was achieved. Prior to the ICP-OES analysis, the samples were appropriately diluted. Certified multi-element standards were employed to verify the accuracy of the calibration and analysis procedures.

3. *Equilibration and quenching of slags*

The equilibration drop-quench experiments were performed inside a vertical tube furnace (Ceramic Engineering, Australia) with $MoSi_2$ elements and an alumina-silicate ceramic work tube. This tube furnace was equipped with brass water-cooled endcaps at both ends of the tube. A calibrated type-B thermocouple (±5 °C error) protruded through the top endcap and a Pt holding wire held the Pt foil capsules containing the slags in the hot zone of the work tube. The bottom end was closed with a thin polypropylene (PP) sheet. The PP sheet was just touching the water surface (room temperature water) of a quenching bath beneath the tube furnace. A frame structure was made with Pt wires to hang multiple Pt capsules inside the hot zone. Figure 1 schematically shows the furnace arrangement for equilibration drop-quench experiments. Once the slag samples reach the equilibration time, the samples were released from the top end of the tube to drop into the water quenching bath and to solidify rapidly to retain the high temperature phase assemblage and structure. The quenched slag samples were immediately transferred to an oven to dry, separated from Pt foils, mounted in epoxy resin in 25 mm round holders and

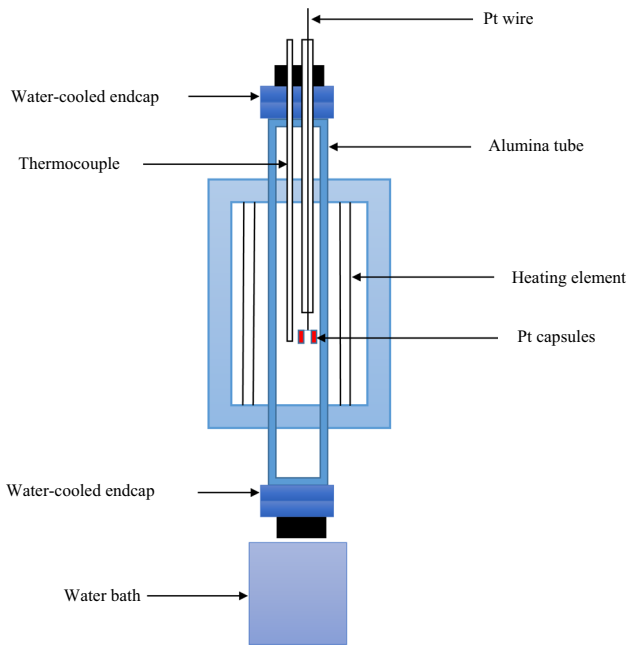

Fig. 1—Schematic diagram of the equilibration drop-quench test furnace and experimental setup (reprinted from previous publications of the same authors)[24,25]

then polished flat using successively finer diamond pastes to expose a cross-section surface of the slag. Precautions were implemented throughout the experimental process to address challenges arising from the hygroscopic nature of Na_2O and B_2O_3 doped slags. To prevent moisture absorption, the prepared slags were consistently stored within desiccators and under vacuum conditions. Even when a water quenching bath was utilized, the quenched samples were promptly transferred to a drying oven to remove any moisture. For characterization purposes, the samples were ground using SiC papers under dry conditions and then polished using a moisture free, oil-based medium to minimize the influence of moisture during the analysis. These measures were taken to ensure the accuracy and reliability of the experimental results by preventing any potential moisture-related complications with the hygroscopic slags. The polished samples were analysed using SEM-EDS and EPMA to determine the equilibrium phase assemblages and the composition of phases. The liquidus temperature of each slag was determined using an iterative approach within ±10–20 °C uncertainty. More detail description of the experimental procedure and characterisation technique can be found in a previously published article.[25]

4. *Characterisation of the quenched slags*

An FEI Quanta 400 SEM equipped with a Bruker EDS system was used to investigate the microstructure and identify the phases present. The SEM analysis was performed using an accelerating potential of 15 kV with a working distance of 10.0 mm. Energy Dispersive Spectroscopic techniques were used to measure the preliminary compositions of the solid and/or liquid phases present and hence identify the crystal phases present in the slag samples. The quantitative analysis of the different equilibrium phases was performed using a JEOL (Model JXA-8500F) electron microprobe. The analysis was performed with an accelerating voltage of 10 kV, a probe current of 5 nA and a beam defocus of 2 μm. The standards used for calibration were wollastonite ($CaO.SiO_2$) for Ca and Si, danburite ($CaB_2Si_2O_8$) for B and spinel ($MgAl_2O_4$) for Al, and albite ($Na_2O.Al_2O_3.6SiO_2$) for Na. For each phase at least 10–15 points were taken, and the average composition was reported along with the standard deviation. Caution was taken to minimize loss of B and Na by evaporation due to the excitement by the electron beam by defocussing the beam and employing short counting times (1 s on the main B peak and 10 s on the background). Also, the low beam current (5 nA) helped reduce potential volatilization. For Na counting times of 6 s on the main Na peak and 3 s on the background were used where for both Al and Ca, it was 20 and 10 s respectively. With this arrangement it was observed that there was negligible boron and sodium loss during analysis as confirmed by repeat analyses. Since boron is very sensitive and lighter it requires more rigorous precautions to reduce uncertainty in analysis. Before analysis, all samples were carbon coated together with the standards to ensure a similar coating thickness so that no additional variable can come from the differential coating thickness.

Equilibration tests were conducted over a range of durations, spanning from 2 to 24 h. Most of the slag samples achieved equilibrium in less than 4 h. However, certain slag compositions, particularly those near the ternary eutectic compositions, experienced difficulties in precipitating a primary phase. To ensure the attainment of equilibrium, two different measurements were employed. First, slag with a specific composition was equilibrated for varying durations to observe if there were any changes in the phase assemblage over time. Second, the compositions of the phases were measured to assess their level of homogeneity. For instance, the S100 master slag was equilibrated at a temperature of 1320 °C for both 4 and 24 h. Upon rapid cooling of the slag from both experiments, only anorthite crystals and a liquid phase were observed, indicating no alteration in the equilibrium phase assemblage with extended duration. Furthermore, a comparison was made between the average compositions of the liquid phase and solid phase from both the 4- and 24-h equilibrated samples. The uniformity of the crystals and the composition of the liquid slag in different locations confirmed that equilibrium was achieved after 4 h of equilibration. This was supported by the fact that there was no significant variation in the composition of the individual phases after a 24-h equilibration period.

III. RESULTS AND DISCUSSION

A. *Composition of the Starting Slag*

The composition of the pre-melted (at 1600 °C) slags used were examined with X-Ray Fluorescence spectroscopy (XRF) and Inductively Coupled Plasma Optical Emission Spectroscopic (ICP-OES) techniques. The results are shown in Table I.

B. *Phase Relations in Equilibrium*

The phase assemblages for the three $CaO\text{-}Al_2O_3\text{-}SiO_2$ master slags and 12 borax doped sub-slags were identified based on the structure and chemistry of the quenched slag samples at different experimental temperatures. Figures 2(a through f) shows a few representative microstructures of the slags and their equilibrium phases captured using the backscattered electron (BSE) imaging mode of SEM. Anorthite ($CaO.Al_2O_3.2SiO_2$) was the primary phase for two of the master slag compositions (S100 and S200) while gehlenite ($2CaO.Al_2O_3.SiO_2$) was the primary phase for the S300 slag. With borax doping of the master slags, the slag system becomes quinary *i.e.*, $CaO\text{-}Al_2O_3\text{-}SiO_2\text{-}Na_2O\text{-}B_2O_3$, and the primary phase field shifts from that of the master slags to another phase field for certain levels of flux addition. Anorthite, pseudowollastonite, gehlenite and sometimes combinations of these primary phases were found to co-exist with their equilibrium liquid. However, no new primary phases were observed within the level of borax doping used (up to 20 wt pct) at the equilibration temperatures close to the liquidus of the

Table I. Composition of the Master Slags and Borax Doped Sub-Slags Used in Quenching Experiments

	Composition (Wt Pct)					
Slag ID	B_2O_3	Na_2O	Al_2O_3	CaO	SiO_2	C/S Ratio
S100	0.0	0.0	18.7	20.0	61.1	0.3
S105NB	3.7	1.7	17.7	19.2	57.8	0.3
S110NB	7.1	3.2	16.6	18.2	54.8	0.3
S115NB	10.7	4.7	15.8	17.3	51.6	0.3
S120NB	14.2	6.3	14.8	16.2	48.4	0.3
S200	0.0	0.0	19.1	29.6	51.0	0.6
S205NB	3.9	1.7	17.7	28.4	48.3	0.6
S210NB	7.3	3.2	16.8	27.0	45.7	0.6
S215NB	10.8	4.8	15.7	25.6	43.1	0.6
S220NB	14.0	6.3	14.9	24.1	40.7	0.6
S300	0.0	0.0	19.1	39.5	41.0	1.0
S305NB	3.7	1.7	17.7	38.0	38.9	1.0
S310NB	7.0	3.1	16.8	36.1	37.0	1.0
S315NB	10.5	4.7	15.8	34.1	34.8	1.0
S320NB	14.1	6.2	14.9	32.1	32.7	1.0

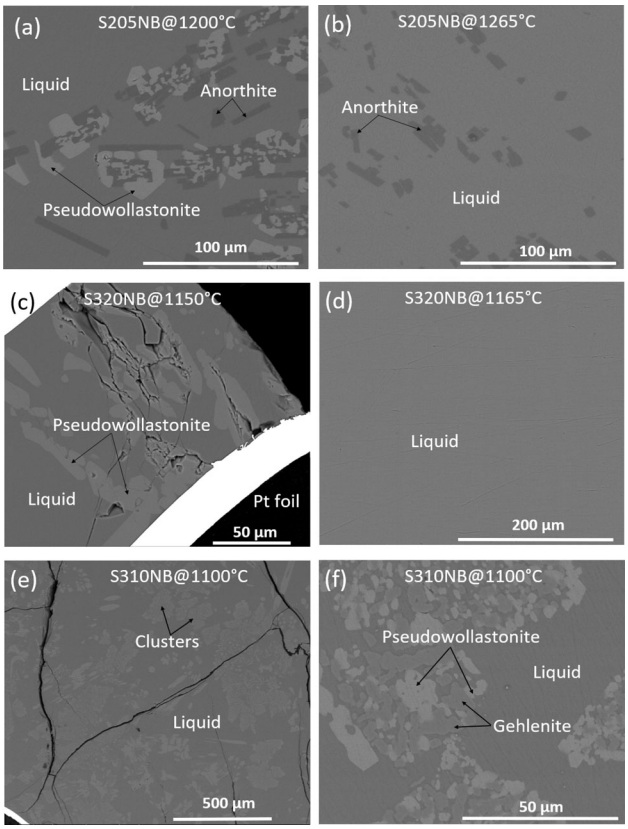

Fig. 2—Representative microstructures showing the phase assemblages of borax-doped CaO-Al_2O_3-SiO_2-Na_2O-B_2O_3 slags (*a*) Anorthite + Pseudowollastonite + Liquid (*b*) Anorthite + Liquid (*c*) Pseudowollastonite + Liquid (*d*) Single liquid phase (*e*) Clusters of multi-solid phases with liquid at low magnification (*f*) Magnified view of the clusters with Gehlenite + Pseudowollastonite + Liquid within the same slag sample.

respective slags. All of the primary crystals reported were present in the ternary CaO-Al_2O_3-SiO_2 phase diagram.[37]

Figure 2(a) shows at equilibrium two solid phases (anorthite and pseudowollastonite) with liquid for slag composition S205NB (5 wt pct borax in slag with C/S ratio 0.6, 17.7 wt pct Al_2O_3) at 1200 °C. With increasing temperature approaching towards the liquidus, anorthite was found to be the primary phase for this slag at 1265 °C (Figure 2(b)), while a single liquid phase exists above 1285 °C. Here, the primary phase remains unchanged with the level of borax doping (5 wt pct). However, the primary phase field can shift to another due to borax doping at different levels. An example of a phase field shifting from gehlenite to pseudowollastonite due to borax doping can be demonstrated with the S320NB slag where the pseudowollastonite primary phase was in equilibrium with liquid at 1150 °C, and a single liquid phase was in equilibrium at or above 1165 °C (Figures 2(c, d)). For the same slag, at lower temperatures, multiple solid phases (gehlenite, pseudowollastonite) were in equilibrium with liquid. The morphology of the solid phases varies from round, hexagonal, long needle shapes for anorthite and pseudowollastonite while gehlenite was found to be irregular in texture. Anorthite typically appears dark and provides good contrast with the liquid phase which contains every element within the slag system. Pseudowollastonite appears bright white since it contains around 48 pct of CaO and 52 pct SiO_2. On the other hand, gehlenite has a very similar contrast with that of the equilibrium liquid phase since the composition of gehlenite crystals are closer to the liquid phase (Table AI, Appendix). In terms of morphology, gehlenites are irregular and sometimes form clusters with pseudowollastonite as can be seen from Figures 2(e, f).

In the course of the iteration process to bracket the liquidus temperature, equilibration-quenching experiments were performed both above and below the liquidus temperatures for each slag studied. At temperatures well below the liquidus, a large amount of crystalline solid phases formed. The phase assemblage at these lower temperatures could be (i) many crystals of a single solid phase co-existing with liquid or (ii) in most cases, crystals of multiple solid phases co-existing with the equilibrium liquid. Sometimes, the density of crystals was so great that they could not grow to a large enough size that could be analysed precisely with EPMA and thus making it difficult to distinguish individual phases. Because of the smaller size (*i.e.*, $<1\mu$m) of crystals in any dimension the interaction volume of the intense electron beam exceeds the crystal volume and thus the beam picks up information from the matrix or adjacent other crystals. Also, the smaller crystal size does not allow for beam defocusing leading to inaccurate quantitative analysis. Similar findings were reported by other researchers.[38] The proportion of solids decreased as the temperature was increased and approached the liquidus for a particular slag composition. Very few primary crystals were observed within the cross section of the quenched slag surface at the lower end of the reported liquidus temperature brackets. A single liquid phase was present at temperatures 10–20 °C above the

highest temperature where the primary solid phase existed in equilibrium with liquid. These liquidus temperature brackets are discussed further in later sections.

The amount of Na in the feldspar increases with the increase of Na in the bulk slag composition and liquid phase (Table AI). Solid solutions within the Ca-Na feldspar series are known as Plagioclase feldspars of which there are a number of different named types within the series e.g anorthite, bytownite, labradorite etc. The classification is based on the level of Na substitution and according to common usage, Anorthite is the correct name for a Ca-Na plagioclase feldspar series mineral with a CaO content >90 pct.[39] Studies by Louisnathan (1970) showed that gehlenite, together with akermanite, forms one of two end member compositions of the melilite series of minerals that have the generalised series formula being $(Ca,Na)_2(Al,Mg,Fe^{2+})[(Al,Si)SiO_7]$, can incorporate the $Na_2Si_3O_7$ molecule *via* solid solution.[40] For calcium and sodium substitution only, the end members of the solid solution series are gehlenite for the Ca-rich end member and $(NaCa)Al_7Si_3O_7$ for the soda melilite endmember.[41] Nurse and Midgley (1953) however showed that the maximum limit of solid solution of potassium melilite in gehlenite was about 20 mole pct.[42]

The EPMA results determined in this study confirm the solid solution incorporation of Na in both anorthite and gehlenite with maximum levels of 3.8±0.5 wt pct (as Na_2O) in anorthite (sample S215NB) and 3.6±0.5 wt pct in gehlenite (S319NB). In other samples Na_2O levels were significantly lower. The small amount of sodium substitution will have an impact on the positions of the primary phase boundaries however at such low levels the effect is considered negligible and within the error of the temperature measurement (*i.e.*, ±10–20 °C).

C. *Effect of Borax on the Liquidus Temperature of Slags*

Liquidus temperatures of the $CaO\text{-}Al_2O_3\text{-}SiO_2$ master slags can be determined from the ternary phase diagrams available in literature. In this study, the liquidus of the three master slags were experimentally measured and compared to accepted literature data. Close agreement between the experimental findings from literature data[37,43] with the present work in terms of the primary phase and their liquidus temperature gave confidence to the accuracy of the method used to study the quaternary and quinary slag systems in this research.

Figures 3 through 5 show the liquidus temperature for the $CaO\text{-}Al_2O_3\text{-}SiO_2\text{-}Na_2O\text{-}B_2O_3$ slags with a C/S ratio of 0.3–1.0 and 15–19 wt pct Al_2O_3 with a nominal borax doping level ranging from 0 to 20 wt pct. Phase assemblages for each slag at temperatures below and above the bracketed liquidus temperature are also shown. At 0 wt pct borax, the solid square shows the liquidus and primary phase from the ternary $CaO\text{-}Al_2O_3\text{-}SiO_2$ slag reported by Rankin and Wright,[37] while the black solid diamonds show the experimentally obtained liquidus and phase assemblage for the same ternary slag system in this study (Figure 3). For the doped experiments, open circles represent temperatures above the liquidus for that particular slag composition

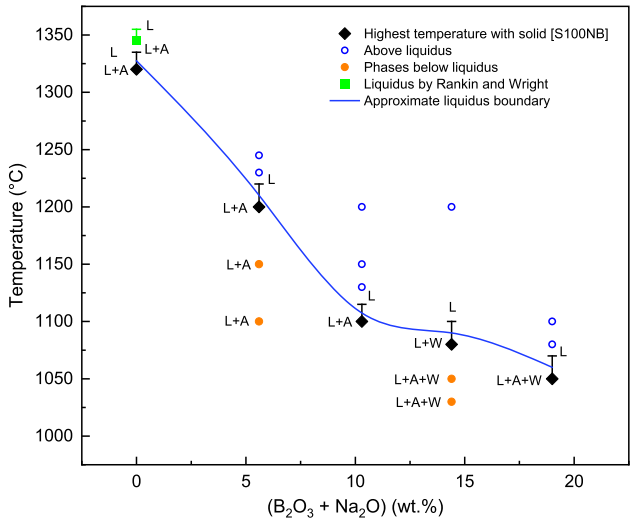

Fig. 3—Change of liquidus temperature and phase assemblages with progressive borax doping in $CaO\text{-}Al_2O_3\text{-}SiO_2\text{-}Na_2O\text{-}B_2O_3$ slags (C/S ratio 0.3, 15–17 wt pct Al_2O_3). L = Liquid, A = Anorthite, W = Pseudowollastonite (the equilibrium composition is provided in Table AI).

while the closed circles indicate temperatures below the liquidus and showing the solid phase/s in equilibrium with the liquid phase. Phases identified are shown beside the closed circles. The error bars shown represent the bracketed liquidus, *i.e.*, the gap between slag samples that were fully liquid and the highest temperature where samples still contained some crystals. Based on equilibration results, the liquidus isotherms for the pseudo-binary systems (C/S ratio 0.3, 0.6 and 1.0) have been estimated as shown in Figures 3 through 5 respectively.

The liquidus isotherm with increasing borax content in the S100 master slag (C/S ratio 0.3) is graphically shown in Figure 3. Overall, the liquidus temperature decreases with increasing levels of borax (represented by $B_2O_3 + Na_2O$ in wt pct) in the slag. The liquidus for the master slag was reported as 1345 °C according to the phase diagram developed by Rankin and Wright. At borax amounts of up to 10 wt pct, the liquidus dropped sharply and linearly reaching 1200 ± 20 °C for 5 wt pct $(B_2O_3 + Na_2O)$ and 1100 ± 15 °C for 10 wt pct $(B_2O_3 + Na_2O)$ doping. Thereafter the degree of liquidus reduction decreased only marginally to 1080 ± 20 °C for 14 wt pct $(B_2O_3 + Na_2O)$ containing slags (S115NB). The lowest liquidus temperature for this series of slag was 1050 ± 20 °C at 19 wt pct $(B_2O_3 + Na_2O)$ addition (S120NB). It was therefore shown that the liquidus temperature of $CaO\text{-}Al_2O_3\text{-}SiO_2$ slags with C/S ratio 0.3 can be reduced by 270 °C by adding nominally 20 wt pct borax in the ternary bulk slag.

The primary phase field of the borax doped slags also changed with an increase of $(B_2O_3 + Na_2O)$ beyond 10 wt pct as shown by the representative microstructures that were discussed in an earlier section (Sect. "Phase Relations in Equilibrium"). Anorthite was the primary phase of the S100 master slag and for slags containing up to 5 and 10 wt pct $(B_2O_3 + Na_2O)$. However, with further addition of borax the primary phase field shifted

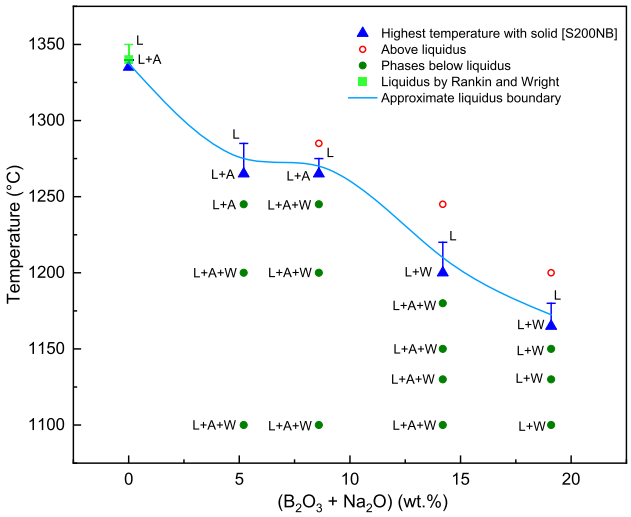

Fig. 4—Change of liquidus temperature and phase assemblages with progressive borax doping in $CaO-Al_2O_3-SiO_2-Na_2O-B_2O_3$ slags (C/S ratio 0.6, 15–17 wt pct Al_2O_3). L = Liquid, A = Anorthite, W = Pseudowollastonite (the equilibrium composition is provided in Table AI).

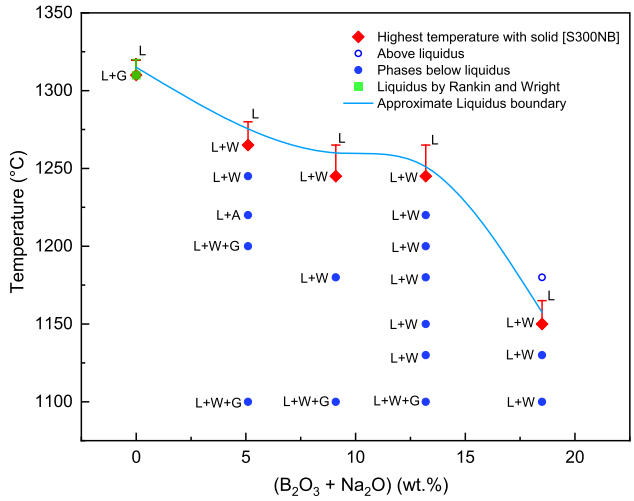

Fig. 5—Change of liquidus temperature and phase assemblages with progressive borax doping in $CaO-Al_2O_3-SiO_2-Na_2O-B_2O_3$ slags (C/S ratio 1.0, 15–17 wt pct Al_2O_3). L = Liquid, A = Anorthite, W = Pseudowollastonite, G = Gehlenite (the equilibrium composition is provided in Table AI).

from anorthite to pseudowollastonite, although at lower temperatures different phase assemblages with multiple solids (anorthite + pseudowollastonite + liquid) were observed as can be seen from Figure 3.

Figure 4 shows the liquidus temperature of the S200 master slag and sub-slags with a C/S ratio of 0.6 and at different borax doping levels. In general, the liquidus temperatures of this slag series decreased with increasing borax content in the slags. The liquidus of the S205NB slag reduced from 1335 to 1265 °C with 5 wt pct ($B_2O_3 + Na_2O$) doping. The change of liquidus then plateaued for the slags doped with 5–9 wt pct ($B_2O_3 + Na_2O$) to around 1265 °C followed by a sharp decline beyond 9 wt pct ($B_2O_3 + Na_2O$) up to 19 wt pct. For the 14 wt pct ($B_2O_3 + Na_2O$) doped slag (S215NB) the liquidus temperature was bracketed to lie within 1200–1220 °C. A further decrease in the slag liquidus to 1165 °C was found with 19 wt pct ($B_2O_3 + Na_2O$) in the liquid slag (S220NB) while at 1180 °C only a single liquid phase existed in equilibrium. In the course of doping, the primary phase field of slags changed along with the liquidus as can be seen from Figure 4. Anorthite was the primary phase for CAS master slag (S200) and continued to be the primary phase up to 9 wt pct ($B_2O_3 + Na_2O$) doped slag. Upon further addition of borax, the primary phase field shifted to pseudowollastonite for the 14 and 19 wt pct ($B_2O_3 + Na_2O$) containing slags. Slags equilibrated at lower temperatures showed more than one solid phase. For example, at 1100 °C, anorthite and pseudowollastonite were in equilibrium with liquid for three of the borax doped slags (S205NB, S210NB and S215NB) while single solid phase pseudowollastonite was in equilibrium for the S220NB slag. When the temperature was increased to close to the liquidus, only the primary phase remained in equilibrium with the liquid phase.

The S300 master slag and sub-slags at a C/S ratio of 1.0, were investigated and the results are summarised in Figure 5 which shows the changes in the slag liquidus with variation in borax content. The experimentally obtained liquidus temperature of the master slag was 1310 °C which was in excellent agreement with that reported by Rankin and Wright.[37] Doping with ($B_2O_3 + Na_2O$) at 19 pct reduced the liquidus from 1310 °C down to 1150 °C. Initially, the liquidus decreased slightly with the addition of 5 wt pct borax and then levelled out with 9–13 wt pct ($B_2O_3 + Na_2O$) addition at 1245 ± 20 °C followed by a more significant reduction of the liquidus with additional (13–19 wt pct) ($B_2O_3 + Na_2O$) addition. Unlike the slag series described previously, the primary phase field changed with the lowest level of ($B_2O_3 + Na_2O$) doping (5 wt pct) from gehlenite to pseudowollastonite and continued up to 19 wt pct ($B_2O_3 + Na_2O$). Several equilibrium tests were run at lower temperatures for each slag, and clusters of gehlenite and pseudowollastonite were observed. Upon increasing the experimental temperatures pseudowollastonite was the only stable phase observed at equilibrium.

D. *Effect of C/S Ratio on the Slag Liquidus*

The CaO/SiO_2 (wt/wt) ratio is a measure of the basicity of the slag system and affects slag properties including liquidus temperature.[44,45] The effect of C/S ratio on the slag liquidus temperature is graphically shown in Figure 6. Here the ($B_2O_3 + Na_2O$) content in the slag ranges from 0 wt pct to 19 wt pct and the Al_2O_3 content changes proportionally within the range of 15 wt pct to 19 wt pct. It is seen that the liquidus temperature increased initially starting from a C/S ratio of 0.3 up to 0.6 for increasing C/S ratio irrespective of the borax doping level. After that, the liquidus slightly

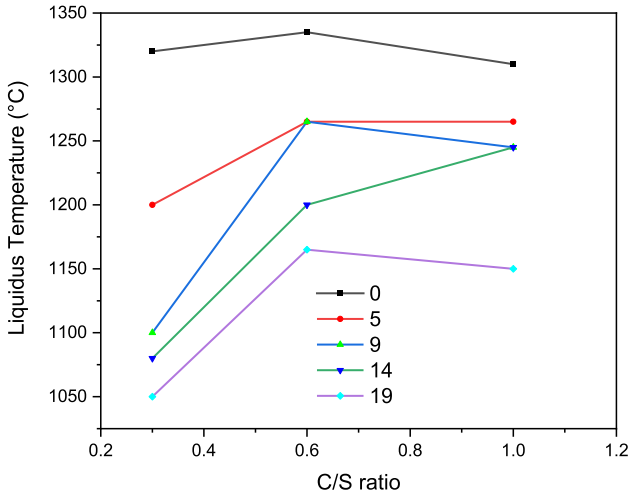

Fig. 6—Variation of slag liquidus temperature with C/S ratio for different flux ($B_2O_3 + Na_2O$) content in slags (up to≈19 wt pct).

reduced with increasing C/S ratio for the slags with 0, 9 and 19 wt pct ($B_2O_3 + Na_2O$) up to C/S ratio 1.0. On the other hand, an increase in liquidus was observed for 14 wt pct ($B_2O_3 + Na_2O$) doped slag from 0.6 up to 1.0 C/S ratio while it plateaued for 5 wt pct ($B_2O_3 + Na_2O$) containing slag when the C/S ratio was increased from 0.6 to 1.0. In this series of slags, the lowest liquidus temperature was attained (when borax was added) for slags having a C/S ratio of 0.3.

E. *Comparison of Liquidus with the Individual Na_2O and B_2O_3 Flux Containing Slags*

For a particular C/S ratio and similar Al_2O_3 content, the liquidus temperature and phase equilibria of CaO-Al_2O_3-SiO_2 based slag changed significantly with different fluxing materials (Na_2O and/or B_2O_3). In previous studies, Na_2O and B_2O_3 were used separately as a flux to reduce the liquidus temperature of the respective quaternary slags[24,25] while in this article a combination of Na_2O and B_2O_3 (sourced from anhydrous borax) was used. The effect of the different levels of these fluxes can be seen from the comparative graphs shown in Figures 7(a through c).

Changes in the liquidus temperature for the S100 series slag (C/S = 0.3) are shown in Figure 7(a) where the liquidus generally decreased with increasing levels of Na_2O, B_2O_3 and ($B_2O_3 + Na_2O$) doping. The lowest liquidus was obtained for this slag series was with B_2O_3 doping, while ($B_2O_3 + Na_2O$) lowered the liquidus slightly less. The liquidus was comparatively higher for the Na_2O doped slags.

For the slag series S200 (C/S ratio 0.6) as shown in Figure 7(b), B_2O_3 fluxing was most effective in lowering the slag liquidus while Na_2O lowers the liquidus to a lesser extent than B_2O_3 but higher than that of ($B_2O_3 + Na_2O$). While the lowest liquidus was around

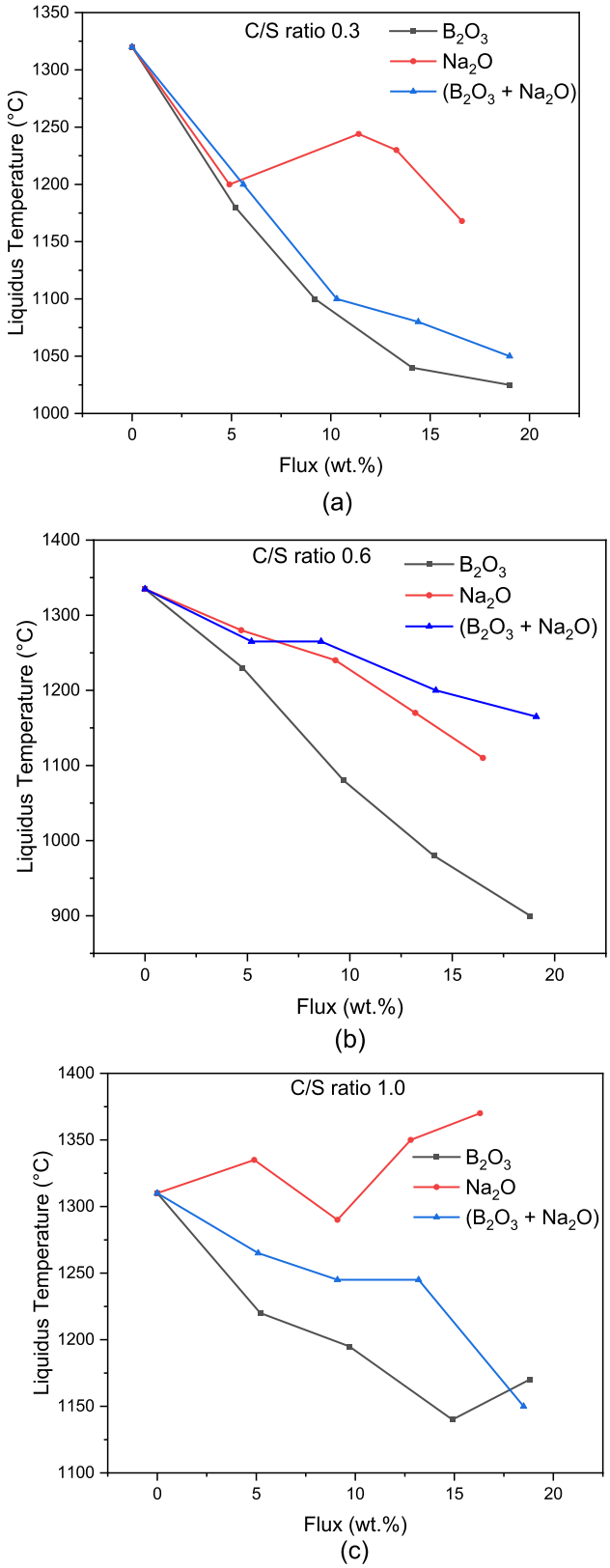

Fig. 7—Comparison of liquidus temperature for slag with different Na_2O, B_2O_3 and ($B_2O_3 + Na_2O$) flux contents with (*a*) C/S ratio 0.3 (*b*) C/S ratio 0.6 and (*c*) C/S ratio 1.0.

900 °C with approximately 19 wt pct B_2O_3, the lowest liquidus achievable with 19 wt pct ($B_2O_3 + Na_2O$) was 1150 °C.

In contrast, doping of Na_2O in the slag series S300 (C/S = 1.0) saw the liquidus temperature increase while the other dopants B_2O_3 and borax caused a decrease in the liquidus with increasing amounts of flux additives. The addition of B_2O_3 lowered the liquidus up to 14 wt pct flux, while further additions of B_2O_3 started to increase the liquidus. The use of ($B_2O_3 + Na_2O$) flux decreased the liquidus continually to at least 19 pct addition. The difference in the shape of the liquidus trend can be attributed to the shifting of the primary phase fields. Sometimes the composition falls on the cotectic boundary between two primary phases in equilibrium as can be seen from the previous research.[24]

Two factors are likely to drive the reduction of slag liquidus. First is the depolymerization of the boroaluminosilicate network structures by the addition of network modifiers such as fluxes e.g., Na_2O. In this case the liquidus temperature decreases with increasing network modifier content within the same primary phase field. The second driving factor is the change in the resultant primary phase after addition of fluxes (borax in this study). In this case, the liquidus temperature could decrease or increase depending on the stability and melting temperature of the primary crystal.

Fluxing $CaO\text{-}Al_2O_3\text{-}SiO_2$ slag with ($B_2O_3 + Na_2O$) reduces the liquidus temperature as evident from the experimental results reported above. Normally, alkali oxides (Na_2O) and alkaline earth oxides (CaO) act as network breakers/modifiers in the binary slag system with pure SiO_2 by creating non-bridging oxygen (NBO).[45,46] With increasing modifier content, they start disrupting the silica network by breaking Si-O-Si bonds and forming Si-O-M bonds and thus impact the physical, chemical and thermodynamic properties including liquidus temperature and viscosity.[47] However, in multicomponent systems where more than one electropositive cation (metal oxide) is present with SiO_2, the system becomes more complex and a number of factors and competing interactions among the cations are in place that need to be considered. For example, Al_2O_3 could be a network former or modifier based on the presence of other surrounding cations which are available to stabilize trivalent Al^{3+} by charge balancing.[48] The role of a particular oxide in the 3D network aluminosilicate and borosilicate structure can be explained by the charge balance mechanism[49] where the stability and equilibrium of the system depends on the electronic charge balance and the surrounding chemical environments. In this mechanism a network modifier (*i.e.*, alkali, alkaline earth oxide) can only contribute to the network breaking if it still remains in the system after charge balancing.[47] The cation acting in charge balancing cannot take part in destabilising the network simultaneously.[50] In this study, due to borax doping, a quinary $CaO\text{-}Al_2O_3\text{-}SiO_2\text{-}B_2O_3\text{-}Na_2O$ system forms where SiO_2, Al_2O_3 and B_2O_3 act as network formers, and CaO and Na_2O act as network modifiers and charge balancers. However, the energetics to form charge balanced four-fold coordinated [$NaAl^{3+}$] is much more favourable compared to [NaB^{3+}].[51,52] If insufficient cations are available to balance B^{3+} they revert to three-fold coordination and compete with SiO_2 for the non-bridging oxygen. This might be the reason why the liquidus temperature of $CaO\text{-}Al_2O_3\text{-}SiO_2\text{-}B_2O_3$ slags of S200B series is the lowest with only B_2O_3 doping and the liquidus is relatively higher (Figure 7) when doped with a mixture of Na_2O and B_2O_3 (borax) where the availability of monovalent alkali Na^+ stabilises [NaB^{3+}] species partly cancels each other from the network modifying role. From the EPMA results it is seen that the doped Na_2O and B_2O_3 remains mostly in the liquid phase and stabilises the liquid phase. Being in the liquid phase these compounds break/modify the silicate bonds to depolymerise the network and thus borax doping reduces the liquidus temperature of slags. However, the extent of liquidus reduction varies with the basicity of the slag generated as denoted by the C/S ratio. Na_2O also increases the slag basicity[49] and Na^+ and Ca^{2+} could play network breaking roles when they remain in the liquid after charge balancing for trivalent Al^{3+} and B^{3+}.

Another reason why the liquidus temperature drops is due to the shifting of the primary phase with progressive doping. While increased doping of fluxes reduces the liquidus within the same primary phase field, a shift from one primary phase to another due to increasing flux content also contributes to a rise or fall in the liquidus depending on the stability and melting temperature of the phase being formed.[25,53] For example, in a previous study, Na_2O doping in the S300 master slag increased the liquidus when the primary phase field shifted towards larnite ($2CaO.SiO_2$) whereas the liquidus dropped due to Na_2O addition in the case of other primary phases.[25]

F. *Significance of the Liquidus Data*

The liquidus temperature of slag is critical for smelting operations. Particularly, it is important to operate smelting processes above the slag liquidus temperature during smelting to assist reaction kinetics as well as to enable better separation of metals and slags. The fluidity of liquid slag also helps to avoid the entrapment of metal prills within the slag. The results presented in this article showed the effect of borax fluxing on the liquidus temperature of $CaO\text{-}Al_2O_3\text{-}SiO_2$ slags which are relevant to smelting of e-waste materials. It is evident that the liquidus temperature drops significantly due to the addition of borax. However,

borax does not contribute to as high a reduction in liquidus temperature as can be obtained from the equivalent use of Na_2O or B_2O_3 separately in some cases. This finding can assist in guiding a choice of flux for smelting processes using these slag systems. Moreover, the experimental liquidus and phase equilibria data can be used to predict phases and liquidus for other complex slags of industrial importance using thermochemical software. Comparative analysis of the effect of different fluxes at different levels will help in the selection of an optimum flux(es) for a range of slag compositions of industrial interest.

IV. CONCLUSION

Phase equilibria and liquidus temperatures of CaO-Al_2O_3-SiO_2 master slags and borax doped CaO-Al_2O_3-SiO_2-Na_2O-B_2O_3 sub-slags with C/S ratio ranging from 0.3 to 1.0 were experimentally investigated by using the well-known equilibration drop-quench method. Anorthite, pseudowollastonite, and gehlenite primary phases along with their equilibrium liquid phase were identified using SEM imaging and the quantitative analysis of phases was performed with EPMA. The primary phase field of the master slags (anorthite and gehlenite) shifted to pseudowollastonite due to different levels of borax doping in three different master slag series. A major proportion of the added B and Na cations from the borax remains in the liquid phase and causes a decrease in the liquidus temperatures of slags at different degrees, while minor amounts of Na and B were found in the solid phases. In general, borax lowered the liquidus temperature for the three series of slags investigated. The highest reduction of liquidus of up to 270 °C was due to 20 wt pct borax doping in the S100 master slag with a C/S ratio of 0.3, while for the S200 slag (C/S = 0.6) it was 170 °C and 160 °C for 20 wt pct borax in the S300 slag (C/S = 1.0). In general, compared to B_2O_3 doping, borax reduces the liquidus of slags at a relatively less pronounced degree. However, borax is more effective compared to Na_2O in reducing the liquidus except for the series with C/S ratio 0.6.

ACKNOWLEDGMENTS

The authors would like to thank Mr. Tom Austin and the Materials Characterization team of CSIRO Mineral Resources for their support to run the experiments and characterise the samples. Also, the financial support provided by CSIRO and RMIT University is acknowledged.

FUNDING

Open access funding provided by CSIRO Library Services.

CONFLICT OF INTEREST

Authors declare that they have no conflict of interest.

APPENDIX: QUANTITATIVE ANALYSIS OF EQUILIBRIUM PHASES OF CAO-AL_2O_3-SIO_2-NA_2O-B_2O_3 SLAG SYSTEM

Table AI shows the chemical composition of phases of the quenched slags equilibrated at different temperatures determined by EPMA. The average composition is reported while the numbers in the parenthesis indicate the standard deviation of the analysis. In most systems multiple solid phases are observed at temperatures significantly lower than the liquidus for a particular slag. In these quenched slags, the proportion of solid crystals were much higher compared to the proportion of liquid phase. The B_2O_3 concentration in this smaller proportion of liquid phase is much higher than that of the liquid phase of the same slag equilibrated at or close to the liquidus temperature. This results from the solid phases preferentially taking Ca, Al, and Si from the melts according to their stoichiometry. As a result, the relative amount of these elements in the liquid phase becomes depleted. Thus, the relative amount of B and Na in the liquid phase increases for a particular slag composition at lower equilibration temperature. For example, in case of S205NB and S305NB the liquid phase contains around 9 wt pct of B_2O_3 at 1100 °C. At their respective liquidus (1265 °C and 1230 °C) the liquid phase of both S205NB and S305NB contains 3.6 wt pct B_2O_3 (Table AI). For a particular slag composition, the boron content in slag is slightly less at higher temperatures than that of lower temperatures. This may be due to the higher evaporation of B from slag melt at higher temperatures during the course of equilibration. Solid crystals (anorthite, gehlenite, pseudowollastonite) contain some of the B and Na in solid solution.

Table AI. Chemical Composition of the Phases of Slags Equilibrated at Different Temperatures Determined by EPMA

Sample ID	Temperature (°C)	Time (Hours)	Phases	Composition (Wt Pct)				
				B_2O_3	Na_2O	SiO_2	CaO	Al_2O_3
S100	1320	22	liquid	0.0 (0.0)	0.0 (0.0)	61.3 (0.2)	20.5 (0.1)	18.2 (0.0)
			anorthite	0.0 (0.0)	0.0 (0.0)	50.6 (0.4)	19.7 (0.3)	29.7 (0.4)
S105NB	1200	4	liquid	3.9 (0.7)	1.7 (0.1)	58.2 (0.3)	19.4 (0.1)	16.8 (0.2)
			anorthite	1.2 (0.7)	2.1 (0.5)	47.0 (0.3)	17.6 (0.2)	32.1 (0.5)
S105NB	1100	4	liquid	3.8 (0.9)	1.5 (0.1)	59.6 (0.6)	20.4 (0.4)	14.8 (0.6)
			anorthite	1.1 (0.8)	1.1 (0.6)	46.3 (0.4)	17.9 (0.3)	33.6 (0.5)
S110NB	1100	4	liquid	7.2 (0.5)	3.1 (0.1)	55.1 (0.6)	18.3 (0.3)	16.3 (0.3)
			anorthite	0.6 (0.5)	1.7 (0.2)	46.9 (0.4)	17.2 (0.3)	33.7 (0.4)
S115NB	1100	4	liquid	9.8 (0.8)	4.6 (0.2)	52.2 (0.6)	17.3 (0.3)	16.1 (0.2)
S115NB	1080	4	liquid	10.2 (0.7)	4.6 (0.2)	51.9 (0.5)	17.3 (0.2)	15.9 (0.2)
			pseudowollastonite	0.6 (0.4)	0.0 (0.0)	51.5 (0.3)	47.7 (0.1)	0.2 (0.1)
S120NB	1100	4	liquid	12.8 (0.8)	6.1 (0.2)	49.8 (0.4)	16.0 (0.2)	15.3 (0.2)
S120NB	1050	4	liquid	13.0 (1.0)	6.1 (0.2)	49.2 (0.6)	16.3 (0.3)	15.5 (0.2)
			pseudowollastonite	0.6 (0.5)	0.0 (0.0)	51.2 (0.3)	48.0 (0.2)	0.1 (0.1)
S200	1335	24	liquid	0.0 (0.0)	0.0 (0.0)	51.5 (0.1)	30.4 (0.1)	18.1 (0.1)
			anorthite	0.0 (0.0)	0.0 (0.0)	44.1 (0.5)	20.2 (0.3)	35.7 (0.4)
S205NB	1265	4	liquid	3.6 (0.8)	1.6 (0.1)	48.4 (0.5)	28.4 (0.2)	17.9 (0.2)
			anorthite	1.1 (0.3)	1.1 (0.1)	45.5 (0.2)	18.5 (0.7)	33.7 (1.2)
S205NB	1100	4	liquid	8.7 (0.6)	2.3 (0.1)	46.5 (0.5)	26.4 (0.2)	16.1 (0.2)
			anorthite	0.5 (0.4)	2.1 (0.3)	47.8 (0.6)	16.9 (0.3)	32.6 (0.9)
			pseudowollastonite	0.7 (0.4)	0.0 (0.0)	51.3 (0.3)	47.7 (0.4)	0.2 (0.2)
S210NB	1265	4	liquid	5.7 (0.5)	2.9 (0.1)	47.1 (0.4)	27.0 (0.2)	17.3 (0.2)
			anorthite	0.0 (0.0)	1.7 (0.2)	47.2 (0.4)	17.3 (0.3)	33.9 (0.3)
S210NB	1100	4	liquid	7.8 (0.8)	3.5 (0.2)	45.5 (1.0)	25.8 (0.4)	17.4 (0.2)
			anorthite	0.9 (0.6)	3.3 (0.2)	50.3 (0.3)	14.4 (0.3)	31.1 (0.3)
			pseudowollastonite	0.6 (0.5)	0.0 (0.0)	51.1 (0.5)	48.2 (0.2)	0.1 (0.0)
S215NB	1200	4	liquid	9.7 (0.5)	4.5 (0.2)	43.9 (0.3)	25.8 (0.1)	16.1 (0.2)
			pseudowollastonite	0.7 (0.5)	0.0 (0.0)	50.6 (0.5)	48.5 (0.3)	0.1 (0.1)
S215NB	1100	4	liquid	9.8 (0.8)	4.6 (0.1)	43.7 (0.3)	25.5 (0.4)	16.5 (0.9)
			pseudowollastonite	0.6 (0.6)	0.0 (0.0)	51.2 (0.4)	48.0 (0.2)	0.1 (0.1)
			anorthite	0.7 (0.6)	3.8 (0.5)	51.2 (1.2)	13.6 (0.8)	30.7 (0.6)
S220NB	1165	4	liquid	13.2 (0.8)	5.9 (0.2)	41.3 (0.2)	24.3 (0.1)	15.2 (0.1)
			pseudowollastonite	0.7 (0.2)	0.0 (0.0)	51.2 (0.4)	48.0 (0.6)	0.1 (0.1)
S220NB	1100		liquid	13.5 (0.6)	6.0 (0.1)	41.1 (0.2)	24.0 (0.2)	15.3 (0.2)
			pseudowollastonite	0.5 (0.0)	0.0 (0.0)	51.4 (0.2)	48.1 (0.0)	0.1 (0.0)
S300	1310	24	liquid	0.0 (0.0)	0.0 (0.0)	41.4 (0.2)	40.1 (0.1)	18.4 (0.1)
			gehlenite	0.0 (0.0)	0.0 (0.0)	23.9 (0.9)	41.6 (0.1)	34.5 (1.1)
S305NB	1265	4	liquid	3.6 (0.6)	1.5 (0.1)	39.1 (0.3)	37.8 (0.1)	18.0 (0.2)
			pseudowollastonite	0.8 (0.5)	0.1 (0.0)	50.7 (0.6)	48.1 (0.1)	0.3 (0.2)
S305NB	1220	4	liquid	3.6 (0.6)	1.6 (0.1)	39.1 (0.4)	37.9 (0.1)	17.8 (0.2)
			gehlenite	1.3 (0.7)	1.9 (0.2)	28.1 (0.9)	37.7 (0.4)	30.9 (0.7)
			anorthite	0.6 (0.6)	0.2 (0.1)	43.1 (0.6)	20.0 (0.1)	36.0 (0.3)
			pseudowollastonite	0.7 (0.4)	0.0 (0.0)	51.1 (0.5)	48.0 (0.1)	0.2 (0.1)
S305NB	1100	4	liquid	9.3 (0.5)	2.8 (0.1)	33.9 (0.3)	34.9 (0.2)	19.1 (0.1)
			gehlenite	2.5 (0.3)	2.6 (0.5)	28.6 (1.2)	37.3 (0.8)	29.0 (1.5)
			anorthite	1.0 (0.6)	0.5 (0.1)	43.6 (0.5)	19.6 (0.4)	35.3 (0.3)
			pseudowollastonite	0.7 (0.6)	0.0 (0.0)	51.0 (0.1)	48.1 (0.1)	0.1 (0.0)
S310NB	1245	4	liquid	6.2 (0.7)	2.9 (0.3)	37.5 (0.4)	36.3 (0.2)	17.2 (0.4)
			pseudowollastonite	0.9 (0.5)	0.0 (0.0)	50.8 (0.7)	48.2 (0.3)	0.1 (0.1)
S310NB	1100	4	liquid	8.4 (0.6)	3.9 (0.1)	35.0 (0.3)	33.0 (0.2)	19.7 (0.2)
			gehlenite	3.7 (0.5)	3.6 (0.2)	30.4 (0.5)	35.6 (0.4)	26.7 (0.3)
			pseudowollastonite	1.6 (0.2)	0.0 (0.0)	49.8 (0.6)	48.4 (0.2)	0.1 (0.0)
S315NB	1245	4	liquid	9.1 (1.0)	4.1 (0.2)	35.9 (0.3)	34.6 (0.2)	16.3 (0.2)
			pseudowollastonite	0.9 (0.2)	0.0 (0.0)	51.0 (0.7)	48.0 (0.1)	0.0 (0.0)
S315NB	1100	4	liquid	9.7 (0.4)	4.7 (0.2)	35.3 (0.4)	34.3 (0.1)	16.0 (0.1)
			pseudowollastonite	0.7 (0.2)	0.0 (0.0)	50.7 (0.9)	48.5 (0.2)	0.0 (0.0)
S320NB	1150	4	liquid	12.4 (0.7)	6.1 (0.2)	33.7 (0.3)	32.5 (0.2)	15.3 (0.2)
			pseudowollastonite	1.3 (0.4)	0.0 (0.0)	50.7 (0.4)	48.0 (0.1)	0.0 (0.0)
S320NB	1100	4	liquid	12.9 (0.7)	5.5 (0.1)	33.4 (0.3)	32.8 (0.1)	16.3 (0.2)
			gehlenite	4.1 (0.9)	3.1 (0.3)	29.6 (0.8)	36.3 (0.6)	26.9 (0.5)
			pseudowollastonite	0.6 (0.4)	0.0 (0.0)	50.9 (0.7)	48.4 (0.1)	0.1 (0.1)

The standard deviation in the solid phase composition was higher compared to the liquid probably because of the topography of the crystals as similar variation was reported in CaO-Al_2O_3-SiO_2 slag system.[54] The liquid phase was found to be homogenous, showing little standard deviation resulting from analytical errors. However, more deviation was observed in the solid phase analysis, which was attributed to topography effects, as reported by other researchers mentioned in the manuscript. Differential hardness of the solid phases compared to the liquid glassy phase during grinding and polishing could cause surface topography. This might lead to uncertainty in measurements, as the electron beam may cover the edges of solid phases and slightly overlap with the glass matrix, due to the micro-scale topographic features of the samples. Ideally, the solid phase compositions should be close to their endmember's stoichiometric composition; however, some elements may remain in solid solution. For instance, the presence of Na in anorthite and gehlenite could cause deviations from their ideal stoichiometric compositions. Also, a relatively higher variation in the B analysis is noticed since B is lighter and higher evaporation under the electron beam causes loss of B even with the cautions taken.

REFERENCES

1. V Forti, CP Baldé, R Kuehr, and G Bel: *Quantities, flows, and the circular economy potential,* 2020, pp. 1–119.
2. F. Cucchiella, I. D'Adamo, S.C.L. Koh, and P. Rosa: *Renew. Sustain. Energy Rev.*, 2015, vol. 51, pp. 263–72.
3. M. Chen, K. Avarmaa, L. Klemettinen, H. O'Brien, D. Sukhomlinov, J. Shi, P. Taskinen, and A. Jokilaakso: *Metall. Mater. Trans. B*, 2020, vol. 51, pp. 1495–1508.
4. V. Jain, S. Kumar, A. Mostofi, and M.A. Momeni: *Waste Manage.*, 2022, vol. 147, pp. 36–47.
5. S. Ilyas, R.R. Srivastava, H. Kim, S. Das, and V.K. Singh: *Waste Manage.*, 2021, vol. 121, pp. 175–85.
6. J. Van Yken, N.J. Boxall, K.Y. Cheng, A.N. Nikoloski, N.R. Moheimani, and A.H. Kaksonen: *Metals*, 2021, vol. 11, p. 1935.
7. X. Zeng, J.A. Mathews, and J. Li: *Environ. Sci. Technol.*, 2018, vol. 52, pp. 4835–41.
8. C. Eswaraiah, T. Kavitha, S. Vidyasagar, and S.S. Narayanan: *Chem. Eng. Process.*, 2008, vol. 47, pp. 565–76.
9. J. Hanafi, E. Jobiliong, A. Christiani, D.C. Soenarta, J. Kurniawan, and J. Irawan: *Procedia-Soc Behav Sci*, 2012, vol. 57, pp. 331–38.
10. L. Zhang and Xu. Zhenming: *J. Cleaner Prod.*, 2016, vol. 127, pp. 19–36.
11. S. Mir and N. Dhawan: *Resour. Conserv. Recycl.*, 2022, vol. 178, p. 106027.
12. H.S. Park, Y.S. Han, and J.H. Park: *ACS Sustain. Chem. Eng.*, 2019, vol. 7, pp. 14119–25.
13. A. Khaliq, M.A. Rhamdhani, G. Brooks, and S. Masood: *Resources*, 2014, vol. 3, pp. 152–79.
14. F. Tesfaye, D. Lindberg, J. Hamuyuni, P. Taskinen, and L. Hupa: *Miner. Eng.*, 2017, vol. 111, pp. 209–21.
15. A. Anindya: Minor elements distribution during the smelting of WEEE with copper scrap, PhD Thesis in RMIT University, Melbourne, Australia (2012).
16. A. Anindya, D.R. Swinbourne, M.A. Reuter, and R.W. Matusewicz: *Miner. Process. Ext. Metall.*, 2013, vol. 122, pp. 165–73.
17. C. Hagelüken: *Erzmetall*, 2006, vol. 59, pp. 152–61.
18. N. Stuart, B. Hogg, O. Mendoza, and S. Nikolic: *Processes*, 2023, vol. 11, p. 1012.
19. Y. Fan, Y. Gu, Q. Shi, S. Xiao, and F. Jiang: in *Advances in Molten Slags, Fluxes, and Salts: Proceedings of the 10th International Conference on Molten Slags, Fluxes and Salts 2016* (Springer, 2016), pp 203–10.
20. R. KokalHarold and M.G. Ranade: *Ind. Miner. Rocks*, 1994, vol. 15, pp. 661–75.
21. A. Baghel, C. Sharma, S. Rathee, and M. Srivastava: *Mater. Today: Proc.*, 2021, vol. 47, pp. 6947–52.
22. P.W.U. Appel and L. Na-Oy: *J Health Pollut.*, 2012, vol. 2, pp. 5–10.
23. I.A. Joseph, E.J. Eterigho, J.O. Okafor, and C.T. Are: *Iran. J. Chem. Chem. Eng.*, 2022, vol. 2021(41), pp. 2288–99.
24. M.K. Islam, M.I. Pownceby, M. Somerville, J. Tardio, N. Haque, and S. Bhargava: *J Sustain. Metall.*, 2022, vol. 8, pp. 1590–605.
25. M.K. Islam, M. Somerville, M.I. Pownceby, J. Tardio, N. Haque, and S. Bhargava: *JOM*, 2021, vol. 73, pp. 1889–98.
26. B. Song, X. Lv, H.H. Miao, K. Han, K. Zhang, and R. Huang: *ISIJ Int.*, 2016, vol. 56, pp. 2140–6.
27. M.H. Morcali, L.T. Khajavi, and D.B. Dreisinger: *Int. J. Miner. Process.*, 2017, vol. 167, pp. 27–34.
28. H. Zhou, K. Feng, Y. Liu, and L. Cai: *J. Non-Cryst. Solids*, 2022, vol. 590, p. 121703.
29. H. Wang, Yu. Keqin Feng, Q.S. Zhou, and H. Shi: *Mater. Lett.*, 2014, vol. 132, pp. 176–8.
30. N. Hui-Teng, H. Cheng-Yong, L. Yun-Ming, M.M. Al-BakriAbdullah, C. Rojviriya, P.W. Ken, O. Shee-Ween, H. Yong-Jie, and O. Wa-n-En: *Constr. Build. Mater.*, 2022, vol. 331, p. 127337.
31. A. Nazari, A. Maghsoudpour, and J.G. Sanjayan: *Constr. Build. Mater.*, 2014, vol. 70, pp. 262–8.
32. https://www.borax.com/products/applications/metals-gold (accessed 20th July 2023).
33. Md Khairul Islam, Nawshad Haque, and Michael A. Somerville: In *TMS 2021 150th Annual Meeting & Exhibition Supplemental Proceedings*, 2021, pp 995-1006.
34. J. Van Yken, K.Y. Cheng, N.J. Boxall, C. Sheedy, A.N. Nikoloski, N.R. Moheimani, and A.H. Kaksonen: *Metals*, 1935, vol. 2021, p. 11.
35. N. Li, E. Vainio, L. Hupa, M. Hupa, and E.C. Zabetta: *Energy Fuels*, 2018, vol. 32, pp. 12971–80.
36. M. Li, T. Utigard, and M. Barati: *Metall. Mater. Trans. B*, 2015, vol. 46, pp. 74–82.
37. G.A. Rankin and F.E. Wright: *Am. J. Sci.*, 1915, vol. 1, pp. 1–79.
38. E. Jak and P.C. Hayes: *Miner. Process. Ext. Metall.*, 2008, vol. 117, pp. 1–7.
39. W.A. Deer, R.A. Howie, and J. Zussman: *An Introduction to the Rock Forming Minerals*, 2nd ed. Longman Scientific & Technical, London, 1992, p. 696.
40. S.J.Z. Louisnathan: *Kristallogr—Cryst. Mater.*, 1970, vol. 131, pp. 314–21.
41. A.D. Edgar: *Can. J. Earth Sci.*, 1965, vol. 2, pp. 596–621.
42. R.W. Nurse and H.G. Midgley: *J. Iron Steel Inst. London*, 1953, vol. 174, p. 121.
43. E.F. Osborn and A. Muan: *Phase equilibrium diagrams of oxide systems*, American Ceramic Society with the Edward Orton Jr Ceramic Foundation, 1960.
44. S. Sadaf, T. Wu, L. Zhong, Z.Y. Liao, and H.C. Wang: *Metals*, 2020, vol. 10, p. 1240.
45. G.-X. Qiu, D.-J. Miao, X.-l Wei, C. Bai, and X.-M. Li: *J. Non-Cryst. Solids*, 2022, vol. 585, p. 121545.
46. J.H. Park, D.J. Min, and H.S. Song: *Metall. Mater. Trans. B*, 2004, vol. 35, pp. 269–75.
47. K.C. Mills: *ISIJ Int.*, 1993, vol. 33, pp. 148–55.
48. H. Hashimoto, Y. Onodera, S. Tahara, S. Kohara, K. Yazawa, H. Segawa, M. Murakami, and K. Ohara: *Sci. Rep.*, 2022, vol. 12, pp. 1–9.
49. A.J.G. Ellison, J.J. Mazer, W.L. Ebert: Effect of glass composition on waste form durability: a critical review, 1994. https://inis.iaea.org/search/search.aspx?orig_q=RN:26047910 (accessed 08 March 2023).
50. K.C. Mills, L. Yuan, Z. Li, G.H. Zhang, and K.C. Chou: *High Temp. Mater. Processes*, 2012, vol. 31, pp. 301–21.
51. J.J. De Yoreo, A. Navrotsky, and D.B. Dingwell: *J. Am. Ceram. Soc.*, 1990, vol. 73, pp. 2068–72.

52. A.J.G. Ellison and P.C. Hess: *J. Geophys. Res.: Solid Earth*, 1990, vol. 95, pp. 15717–26.
53. B. Zhao, P.C. Hayes, and E. Jak: *Miner. Process. Extr. Metall.*, 2013, vol. 121, pp. 32–39.
54. E. Haccuria, T. Crivits, P.C. Hayes, and E. Jak: *J. Am. Ceram. Soc.*, 2016, vol. 99, pp. 691–704.
55. M. Nakamoto, Y. Miyabayashi, L. Holappa, and T. Tanaka: *ISIJ Int.*, 2007, vol. 47, pp. 1409–15.